Photo-production of the Higgs boson at the LHeC

Ruibo Li, Xiang Lv, Bo-Wen Wang [*], Kai Wang, Tao Xu

Zhejiang Institute of Modern Physics and Department of Physics, Zhejiang University, Hangzhou, Zhejiang 310027, China

Abstract

As one category of vector boson fusion, photo-production is one important production mechanism at e-p colliders. A future e-p collider – Large Hadron-electron Collider (LHeC) has been discussed as a "Higgs factory" candidate where the Higgs boson produced via weak boson fusion (WBF) at the LHeC plays an important role in precision measurement of Yukawa couplings. On the other hand, a measurement of photo-production of the Higgs boson, if possible, might be complementary to the measurement of Higgs to di-photon partial decay width $\Gamma(h \rightarrow \gamma\gamma)$. In this paper, we study the possibility of measuring this production process at the LHeC with the help of the photon PDFs published in recent years. This process has a clean final state without additional colored particles in the detectable region other than the decay products of the Higgs. We compute the cross sections of all related processes and find that the production rate is at the same order as the neutral current WBF production of Higgs boson with missing forward jets. However, a detailed phenomenological study of various Higgs decay channels shows that even in the most promising semi-leptonic WW channel, the feasibility of identifying such photo-production is negative due to an irreducible photo-production of W^+W^-.

* Corresponding author.
 E-mail addresses: bobli@zju.edu.cn (R. Li), lvxiang@zju.edu.cn (X. Lv), 0617626@zju.edu.cn (B.-W. Wang), wangkai1@zju.edu.cn (K. Wang), taoxu.4@gmail.com (T. Xu).

1. Introduction

The discovery of a 125 GeV Standard Model (SM) like Higgs boson by the ATLAS and CMS collaborations at the CERN Large Hadron Collider (LHC) [1,2] has significantly improved our knowledge over the mechanism behind spontaneous electroweak gauge symmetry breaking. On the other hand, neither the mass of the Higgs boson nor the driving force of electroweak symmetry breaking is explained within the SM and these questions have motivated many attempts in extending the SM. Besides the direct search of such models of physics beyond SM (BSM), precision measurement of Higgs boson couplings and properties at the same time plays an important role in testing various BSM physics models. For this purpose, proposals of future electron-positron colliders, such as, FCC-ee, ILC and CEPC, have been widely discussed in the community. Besides them, there also exists a proposal for an e-p collider known as the Large Hadron-electron Collider (LHeC), planned to be constructed by adding an electron beam of 60-140 GeV to the current LHC [3]. LHeC was initially proposed as a TeV deep-inelastic scattering (DIS) facility with 60 GeV electron beam and 2 ab^{-1} designed integrated luminosity to improve the measurement of parton distribution functions at large Bjorken x. By upgrading the electron beam energy and designed luminosity, it can potentially be converted into a "Higgs factory". The leading production mode of Higgs boson at the LHeC is via charged-current weak boson fusion (WBF): $e + p \rightarrow \nu_e + h + j$. The tagged forward jet is found to be crucial for suppressing the background in studies on the $hb\bar{b}$ and $hc\bar{c}$ couplings at the LHeC [4,5]. Analogous to the use of jet angular correlation in measuring the anomalous coupling in WBF at the LHC [6], the azimuthal angle between the neutrino and forward jet $\Delta\phi_{\not{E}_T J}$ provides a sensitive probe of the anomalous hWW coupling at the LHeC [7].

The diphoton decay of Higgs boson played an important role in the Higgs discovery at the LHC. At leading order, the SM Higgs decay into diphoton ($h \rightarrow \gamma\gamma$) arises from the W-loop and heavy quark loop processes, where the W-loop dominates the decay width. Exotic particles from BSM models such as sfermions in supersymmetric models or charged Higgs in the extended Higgs sector may also contribute to the diphoton decay at one-loop level. Therefore, the loop-induced diphoton decay provides a sensitive probe to physics at TeV scale. On the other hand, the photon-fusion production rate of Higgs boson is proportional to the Higgs diphoton decay width. Therefore, precision measurement of the photon-fusion process could potentially be complementary to the diphoton decay measurement.

Recent developments of photon PDF from CT14qed/LUXqed/NNPDF23qed [8–11] have improved our framework for computing photon initiated processes. While the photon radiation off a point-like particle e.g. electron can be calculated explicitly or sometimes with Weizsäcker-Williams approximation, photons from the proton can arise from both elastic and inelastic processes. The elastic channel contribution is from photons directly radiated off a proton, while the inelastic channel is from those radiated off partons. To verify the photon PDF results, the exclusive muon pair production via $\gamma\gamma \rightarrow \mu^+\mu^-$ has been measured for the first time by CMS [12]. One complication in measuring Higgs photo-production at e-p colliders is that the gluon fusion production of Higgs boson contributes in e-p collisions through γg scattering. In addition, the contribution from WBF process with untagged forward partons may not be neglected either. Hence, in order to explore the proton-production at the LHeC, the complete calculation and analysis of all these processes are important.

The paper is organized as follows. In the next section, we discuss the Higgs photo-production process and its cross section at the LHeC. In section 3, we will study the features of the signal,
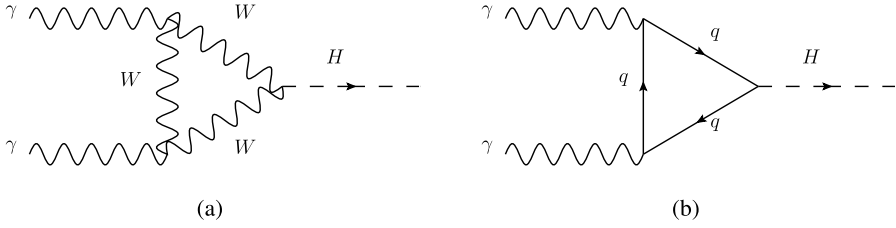
Fig. 1. Representative Feynman diagrams of the Higgs photo-production. q denotes any charged fermions. Top and bottom quark are dominant in the fermion loop.

Table 1
Cross sections in fb for processes represented by the diagrams in Fig. 1, computed with three different PDF sets. The electron beam energy is 60/120 GeV.

Fig. 1	NNPDF23qed	CT14qed_inc	LUXqed17
$E_e = 60$ GeV	0.52	0.39	0.46
$E_e = 120$ GeV	0.74	0.64	0.74

classify the background processes and carry out a phenomenological analysis to separate the signal and backgrounds. The results will be shown and briefly discussed in the last section.

2. Higgs photo-production process at the LHeC

The Feynman diagrams of the Higgs photo-production process through W and charged fermion loops are shown in Fig. 1. The photons are radiated from the proton and electron beams. As the proton remnant has little recoil in the effective photon approximation [13], it moves in the very forward direction and may even escape the detector. The process is therefore featured with its clean final states without additional colored particles.

The photo-production cross sections are summarised in Table 1 for two electron beam energies. For comparison we list the result computed with `NNPDF23_nlo_as_0119_qed` [8], and two more recent PDF sets `CT14qed_inc_proton` [9] and `LUXqed17_plus_PDF4LHC15_nnlo_100` [10,11], obtained from the LHAPDF6 [14]. These cross sections differ by a sizable amount because the methods in determining these photon PDFs are quite different. The LUXqed17 result is smaller than NNPDF23qed at large momentum fraction x, while gets close when x becomes smaller ($\sim \mathcal{O}(10^{-2})$). The CT14qed_inc cross section is smaller than LUXqed17 in a more broad x region. These observations are in qualitative agreement with the behaviors of the photon PDFs shown in Fig. 4 of the Ref. [10].

The results above are obtained with the full electron-photon splitting process considered. One could also carry out the calculation using Weizsäcker-Williams approximation [13]. This approach gives for instance, a cross section of 0.48 fb, for $E_e = 60$ GeV, with NNPDF23qed. The accuracy of the approximation is satisfactory.

3. Phenomenological analysis

In this section we study the possible background processes for the Higgs photo-production signal, and how to suppress them. There are two classes of backgrounds, those with and without
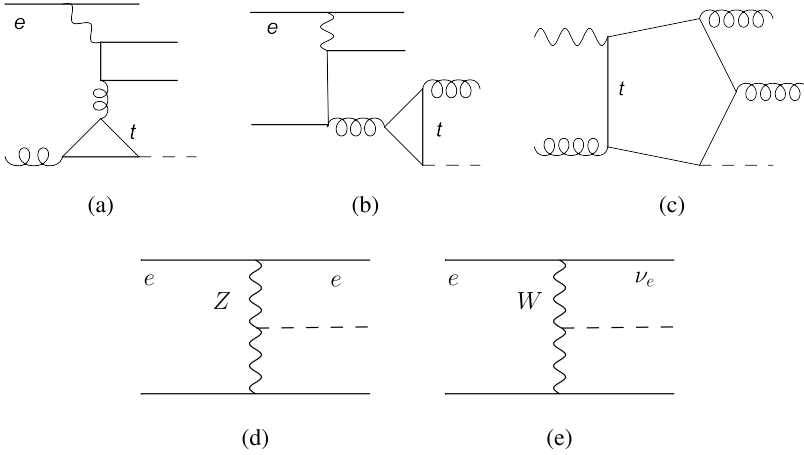
Fig. 2. Representative Feynman diagrams for the backgrounds with a Higgs produced. The electron lines in (a) and (b) indicate that Weizsäcker-Williams approximation for photon radiations is not applicable in these cases and the electron-photon vertices are included explicitly in the calculation.

a Higgs boson produced. The former ones will, of course, appear in all Higgs decay channels. This allows a study of the Higgs production subprocess without considering its decay, which will be done in section 3.2. On the other hand, processes without an intermediate Higgs may also produce final states that mimic the Higgs decay product in various decay channels. However, the background contamination in this case will differ channel by channel. We shall discuss this class of backgrounds in section 3.3 along with the simulation of the Higgs decays.

3.1. Forward electron tagging

In the Higgs photo-production process, one expects to observe only the decay product of the Higgs in the central rapidity region. The forward final state electron is usually assumed to escape from the detector because of its large pseudo-rapidity η. However, with the forward detector at the LHeC [3], abundant forward electrons from signal events would be visible. In this case, the forward electron tagging can also be an important method to separate the photo-production from other processes. An ongoing study [15] shows that in photo-production processes nearly half of the electrons fall into the region $|\eta| \leq 5$. We could do this tagging to remove all backgrounds with no scattered forward electrons in the final state, e.g. charged current WBF. The result of the forward electron tagging for various backgrounds will be shown in our analysis below.

3.2. Backgrounds with a Higgs produced

The Backgrounds with a Higgs produced have a common characteristic that their final state partons (other than those from the Higgs decay) are too soft or collinear to the beams to be tagged. Such processes, as shown in Fig. 2, can be irreducible backgrounds. In particular, there are gluon initiated processes with more radiations. With the increasing energy, the contribution from gluon PDF may quickly result in sizable background cross sections. Therefore, these processes should not be simply ignored without knowing their contributions. In the following, we classify processes with their initial states and discuss the corresponding cross section calculations.

Table 2
Cross sections in fb for processes represented by the diagrams in Fig. 2(a), (b), and (c), computed with three different PDF sets. The electron beam energy is 60/120 GeV.

$E_e = 60$ GeV	Fig. 2(a)	Fig. 2(b)	Fig. 2(c)
NNPDF23qed	~0.017	$\sim 7.5 \times 10^{-4}$	1.9×10^{-4}
CT14qed_inc	~0.016	$\sim 7.6 \times 10^{-4}$	2.0×10^{-4}
LUXqed17	~0.017	$\sim 8.2 \times 10^{-4}$	2.0×10^{-4}
$E_e = 120$ GeV	Fig. 2(a)	Fig. 2(b)	Fig. 2(c)
NNPDF23qed	~0.038	~0.0016	7.8×10^{-4}
CT14qed_inc	~0.035	~0.0016	8.1×10^{-4}
LUXqed17	~0.034	~0.0018	8.1×10^{-4}

3.2.1. $\gamma g / \gamma q \to hX$

The process represented by Fig. 2 (a) also has a clean final state in which hadrons with small rapidities come from the Higgs decay, despite the presence of additional radiation of the quark pair. In fact, when the electron and quark masses m_e and m_q are much smaller than the center-of-mass energy $\sqrt{s}$, the strongly ordered multiple splittings from Fig. 2 (a) give terms proportional to

$$\alpha_{EM}^2 \alpha_S \left[\ln^3\left(\frac{s}{m_e^2}\right) - \ln^3\left(\frac{m_q^2}{m_e^2}\right) \right]. \tag{1}$$

These triple logarithms could substantially enhance the cross section in the region where the quark pair is collinear to the electron. Because of this enhancement, the cross section from this channel receives large contribution from the outgoing electron in the very forward region. In principle, one could represent the structure of the electron by parton distribution functions that evolve to account for the effects of the large logarithms to all orders. However, as we shall see, the cross section of this channel turns out to be quite small. We therefore ignore processes with more radiations and perform an order-of-magnitude estimation using only the diagrams in e.g. Fig. 2 (a), whose collinear singularities are cut off by the electron mass. Also note that due to the multi-logarithmic structure of radiations, Weizsäcker-Williams approximation cannot be used in this case, since additional collinear singularities exist in the hard scattering process even after the electron splitting vertex is factorized. We therefore include the electron line in Fig. 2 (a) to indicate that the exact electron-photon vertex is included in the calculation. The phase space integration of this channel is subject to large numerical uncertainty due to the rapid increase of the scattering amplitude in the collinear region.

Similar to the case in Fig. 2 (a), the quark radiation in Figs. 2 (b) is also enhanced, but with more mild double logarithms of the form

$$\alpha_{EM}^2 \left[\ln^2\left(\frac{s}{m_e^2}\right) - \ln^2\left(\frac{m_q^2}{m_e^2}\right) \right]. \tag{2}$$

In contrast, the gluon radiations from Fig. 2 (c) are not enhanced at large rapidities of the final gluons, in which case single logarithms $\alpha_{EM} \ln(s/m_e^2)$ appear as prescribed by Weizsäcker-Williams approximation. Note that one cannot invoke Furry's theorem to discard the pentagon graphs for two obvious reasons: the number of γ matrices from the vertices in the loop is even; and there is a mixing of QED and QCD vertices.

Table 3

Cross sections in fb for processes represented by the diagrams in Fig. 2(d) and (e), computed with three different PDF sets. The electron beam energy is 60/120 GeV.

$E_e = 60$ GeV	Fig. 2(d), $|\eta^q| \geq 5$	Fig. 2(e), $|\eta^q| \geq 5$
NNPDF23qed	0.68	4.8
CT14qed_inc	0.69	5.0
LUXqed17	0.70	4.9
$E_e = 120$ GeV	Fig. 2(d), $|\eta^q| \geq 5$	Fig. 2(e), $|\eta^q| \geq 5$
NNPDF23qed	1.08	7.5
CT14qed_inc	1.09	7.6
LUXqed17	1.10	7.6

The cross sections for γg and γq processes are shown in Table 2, where the "∼" indicates the number is presented with large uncertainty and serves only as an order-of-magnitude estimate, for the reason discussed above. The three PDF sets give very close results. These cross sections are at most ∼ 5% of that of the photo-production at the energies we are considering. Hence, we will neglect the contributions from the diagrams (a), (b) and (c) in Fig. 2.

3.2.2. Weak boson fusion

WBF processes as in Fig. 2 (d) and (e) are the dominant for Higgs production at the LHeC with a large cross section of $\mathcal{O}(10^2)$ fb. Therefore we expect some rate from the WBF processes without spectator partons (those not from Higgs decay) in the detectable region. To calculate the cross section we exclude the region $|\eta^q| \leq 5$,[1] where q denotes the final state quark (not from Higgs decay). There is again little PDF dependence for the cross sections shown in Table 3. The neutral current WBF cross sections are comparable to those of the photo-production, while the charged current ones are about an order of magnitude larger. However, the charged current process can be eliminated completely by forward electron tagging as discussed in Sec. 3.1. Therefore, we will not consider it in our following simulation.

Throughout this paper we choose the renormalization and factorization scales to be the center-of-mass energy for the hard scattering processes. The reduction of the pentagon loop integral in Fig. 2 (c) requires extra numerical accuracy and is done with the help of Madloop program [16] in *MadGraph5_aMC@NLO* [17]. Other loop diagrams are calculated with FormCalc and Loop-Tools [18]. The Monte Carlo phase space integration is performed using VEGAS algorithm implemented in CUBA library [19].

3.3. Simulation and selection cuts

In this part we explore the possibility of separating the Higgs photo-production—to be taken as our signal process—from other backgrounds with similar final states. The final state particles from the background can be produced from the Higgs decay after the processes shown in Fig. 2. On the other hand, there are backgrounds from γg and $\gamma \gamma$ scatterings that can produce final states similar to those from various Higgs decay channels. To separate all these backgrounds from the signal we make use of the kinematic features of three main decay channels ($h \to b\bar{b}$, W^+W^- and

---

[1] We do not do this for γq and γg processes because their cross sections are negligible already.

ZZ). The background simulation is performed with *MadGraph5_aMC@NLO* [17] at the parton level, and we use *Pythia6.420* [20] and *Delphes3.3.0* [21] for parton shower and detector simulations respectively. The PDF set `NNPDF23_nlo_as_0119_qed` is used in simulations of both the signal and backgrounds, which includes both elastic and inelastic photon information [8]. As is done in Sec. 2, we choose two benchmark electron beam energies at 60 GeV and 120 GeV with 7 TeV proton beam to see whether increasing the electron beam energy helps to improve the Higgs production measurement. The basic cuts on final states p_T, η and ΔR are applied as

$$p_T^\ell \geq 5 \text{ GeV} , \ p_T^j \geq 20 \text{ GeV},$$
$$|\eta^\ell| \leq 5 , \ |\eta^j| \leq 5,$$
$$\Delta R_{\ell\ell} \geq 0.4 , \ \Delta R_{jj} \geq 0.4, \tag{3}$$

where l and j denote a final state lepton and parton respectively.

3.3.1. $b\bar{b}$

The standard $h \rightarrow b\bar{b}$ search at the LHeC uses forward jet tagging to improve the signal-to-background rate, which makes possible the bottom Yukawa measurement [4]. In our search the main background processes are $\gamma g \rightarrow b\bar{b}$ and $\gamma g \rightarrow c\bar{c}$, with c misidentified as b in the detector. The large difference between gluon and photon PDFs in the proton makes the background cross-section orders larger than that of the signal. In order to pick out the signal events, the b-jet transverse momentum could be used because the b quarks from Higgs decay are more boosted. The $b\bar{b}$ invariant mass is another discriminative kinematic variable and only events with $m_{b\bar{b}}$ around m_h should be kept. The $b\bar{b}$ search efficiency also depends heavily on the b-tagging (ϵ_b) and c faking ($\epsilon_{c\rightarrow b}$) efficiencies of the detector. Here we assumed $\epsilon_b = 70\%$ and $\epsilon_{c\rightarrow b} = 20\%$ [22]. The signal production cross section is about 0.148 fb for $E_e = 60$ GeV and 0.211 fb for $E_e = 120$ GeV with $Br(h \rightarrow b\bar{b}) \approx 58\%$. However, the $b\bar{b}$ background cross sections for the two energies are 92.1 pb and 151.2 pb, and the misidentified $c\bar{c}$ backgrounds are 31.7 pb and 52.1 pb. Even after we apply kinematic cuts on the invariant mass of two b jets — m_{bb}, the larger transverse momentum of the two b jets — $^1 p_T^b$, and $\Delta\eta = |^1\eta^b -^2 \eta^b|$ as shown in Fig. 3, about 6% of the total background events could survive. This is still several orders larger than the raw signal events. For this reason, it's extremely challenging to use $b\bar{b}$ channel for this measurement.

3.3.2. W^+W^-

The W^+W^- channel is the secondary Higgs decay channel with $Br(h \rightarrow W^+W^-) \approx 21.5\%$. In this study, we consider the semi-leptonic W decay, in which one W boson decays to $\ell\nu_\ell$ ($\ell = e, \ \mu$) and the other to hadronic final states (two jets jj). Note that in the pure leptonic W decay channel there is huge background from γg and $\gamma\gamma$ scatterings, while the corresponding background for the semi-leptonic W decay is much more moderate. There can be the background from $\gamma\gamma \rightarrow \tau^+\tau^-$ with the semi-leptonic decay of the τ's. However, the low invariant mass of the two jets from a τ decay can be easily distinguished from that in the decay of a W. Hence, we shall neglect the contamination from the τ decay. The main background will be from $\gamma\gamma \rightarrow W^+W^-$ with the semi-leptonic W decay. There is also the background from $\gamma g \rightarrow qq'\ell\nu_\ell$, with two quarks q and q', a lepton ℓ and a neutrino ν_ℓ produced. As discussed before, the neutral current WBF process with forward spectator partons will be another background. We present the analysis of this channel in two methods.
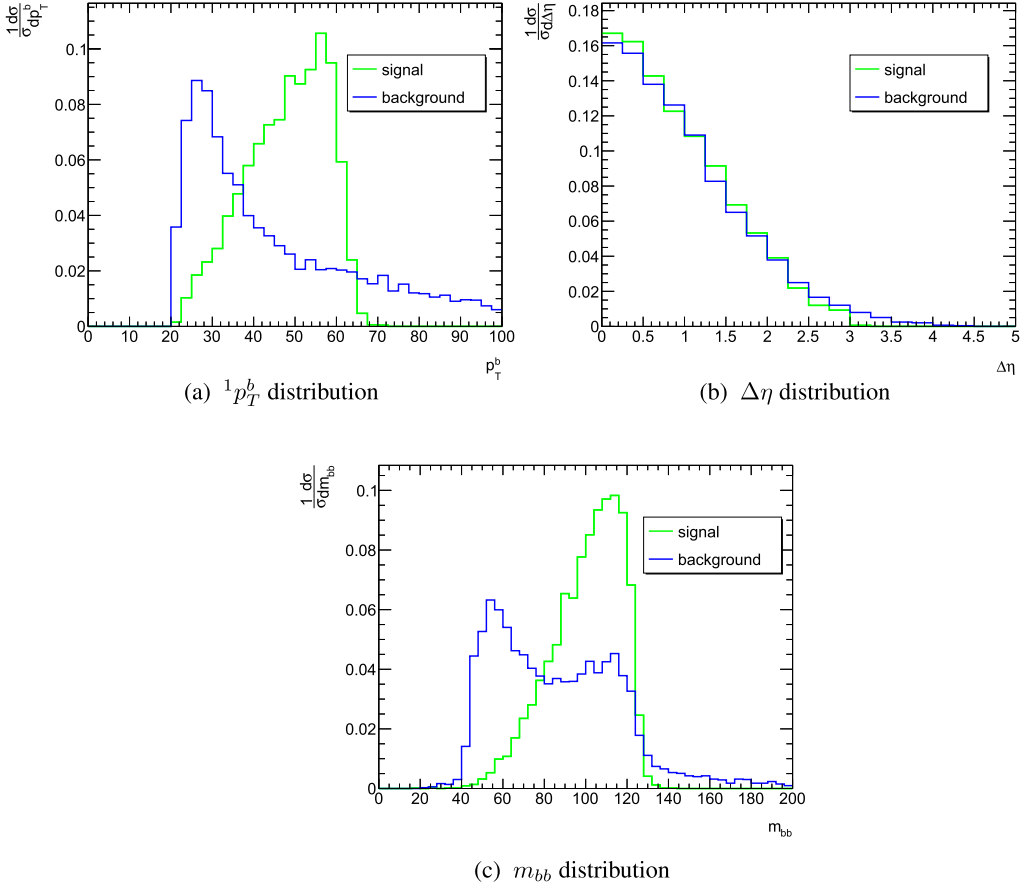
(a) $^1 p_T^b$ distribution

(b) $\Delta \eta$ distribution

(c) m_{bb} distribution

Fig. 3. (a), (b) and (c) are distributions of $^1 p_T^b$, $\Delta \eta$ and m_{bb} for the signal (green) and background (blue), reconstructed from events after basic cuts. The electron beam energy is $E_e = 60$ GeV. (For interpretation of the colors in the figure(s), the reader is referred to the web version of this article.)

The signal and background processes all produce neutrinos that lead to $\not{E}_T$. Though it's very difficult to reconstruct invariant masses involving neutrinos, kinematic methods for the intermediate-mass Higgs boson search could be applied in this case [23]. The $jj\ell\not{E}_T$ system transverse mass could be reconstructed with the transverse momenta of the jets, leptons and the missing objects as

$$
\begin{aligned}
m_T^2 &\equiv (E_T^{jj\ell} + \not{E}_T)^2 - |\mathbf{p}_T^{jj\ell} + \not{\mathbf{p}}_T|^2 \\
&= (\sqrt{|\mathbf{p}_T^j + \mathbf{p}_T^j + \mathbf{p}_T^\ell|^2 + m_{jj\ell}^2} + |\not{\mathbf{p}}_T|)^2 - |\mathbf{p}_T^j + \mathbf{p}_T^j + \mathbf{p}_T^\ell + \not{\mathbf{p}}_T|^2
\end{aligned}
\tag{4}
$$

The signal transverse mass distribution has an upper bound at m_h, while the background distribution can be rather flat. Fig. 4 (a), (d) and (e) show the distributions of $jj\ell\not{E}_T$ system transverse mass, the missing transverse energy and the final lepton transverse momentum. They display a typical distinction between the photo-production signal and the backgrounds. In the signal process, the photon radiations are largely enhanced in the kinematical region collinear to the incoming beams, which results in the Higgs produced with little transverse motion. Hence, the
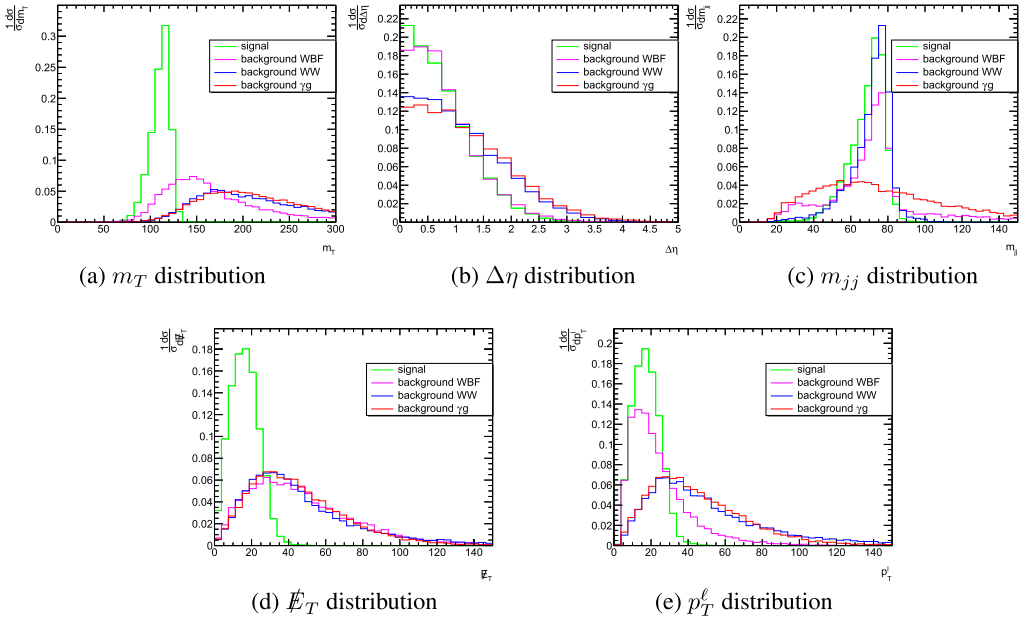
Fig. 4. (a) (b) and (c) are distributions of m_T, $\Delta\eta$, and m_{jj} for the signal (green) and background (magenta, blue and red), reconstructed from events after basic cuts. Distributions of $\not{E}_T$ and p_T^ℓ are shown in (d) and (e). The electron beam energy is $E_e = 60$ GeV.

m_T, $\not{E}_T$, and p_T^ℓ of the decay product also remain small. In contrast, the collinear enhancement in neutral current WBF process is much weaker because of the large Z mass. The W^+W^- and γg backgrounds are produced via radiations of collinear photons and/or gluons. However, unlike the case of the signal, the transverse motion of their final states is not restricted by the virtuality of intermediate Higgs particles. This explains the long tails of the background distributions in these figures. It's reasonable to set upper bounds for these observables to cut the background. As the signal lepton and two central jets are from the Higgs cascade decay, the pseudo-rapidity difference $\Delta\eta$ between them should be smaller than backgrounds. One can see in Fig. 4 (b), and (c) that the pseudo-rapidity difference and the invariant mass of the two jets could be effectively used to distinguish the signal and background. The kinematic distributions are not significantly dependent on the electron beam energy, so we only plot the $E_e = 60$ GeV case.

According to the discussion, we require $\not{E}_T \leq 30$ GeV, $p_T^\ell \leq 30$ GeV, $\Delta\eta \leq 2.5$, 45 GeV $\leq$ $m_{jj} \leq 85$ GeV and $m_T \leq 125$ GeV. The efficiencies of signal and background events after all these cuts are listed in Table 4. Tagging the forward electron removes the charged current WBF background completely, but it also significantly reduces the signal, which makes the measurement more difficult. Whether we perform the electron tagging or not, the signal is overwhelmed by the background, even though the kinematic cuts can reduce the background by about two orders.

The cut efficiencies above can be improved by performing a multivariate analysis with boosted decision trees (BDT). We carry out this analysis in the TMVA [24] framework. Our initial selection of events imposes the same basic cuts as above, and requires at least one lepton ℓ and two jets jj in the final states. Then the following kinematic variables are used to train the BDT for the semi-leptonic final states. They are the p_T, ϕ, and E of the leading jet, sub-leading jet and

Table 4
The second column gives the cross sections of the signal and background after basic cuts. Other columns are cut efficiencies after corresponding kinematic cuts. Background WBF denotes the background from the neutral current WBF process in Fig. 2. The electron beam energy is 60/120 GeV.

| $E_e = 60$ GeV	Cross section (fb)	Forward electron tagging	$p_T^\ell \leq 30$ GeV	$\not{E}_T \leq 30$ GeV	$|\Delta\eta| \leq 2.5$	$m_T \leq 125$ GeV	45 GeV $\leq m_{jj} \leq 85$ GeV
Signal	3.3×10^{-2}	0.48	0.46	0.44	0.44	0.42	0.41
Background WBF	4.3×10^{-2}	0.55	0.40	0.13	0.12	0.071	0.061
Background W^+W^-	53.9	0.50	0.15	0.026	0.021	0.011	0.011
Background γg	12.9	0.50	0.16	0.025	0.020	0.0078	0.0064
$E_e = 120$ GeV	Cross section (fb)	Forward electron tagging	$p_T^\ell \leq 30$ GeV	$\not{E}_T \leq 30$ GeV	$|\Delta\eta| \leq 2.5$	$m_T \leq 125$ GeV	45 GeV $\leq m_{jj} \leq 85$ GeV
Signal	4.7×10^{-2}	0.48	0.46	0.44	0.44	0.42	0.42
Background WBF	6.9×10^{-2}	0.55	0.39	0.15	0.13	0.071	0.056
Background W^+W^-	93.1	0.50	0.15	0.026	0.020	0.010	0.010
Background γg	32.9	0.50	0.16	0.025	0.019	0.0078	0.0058
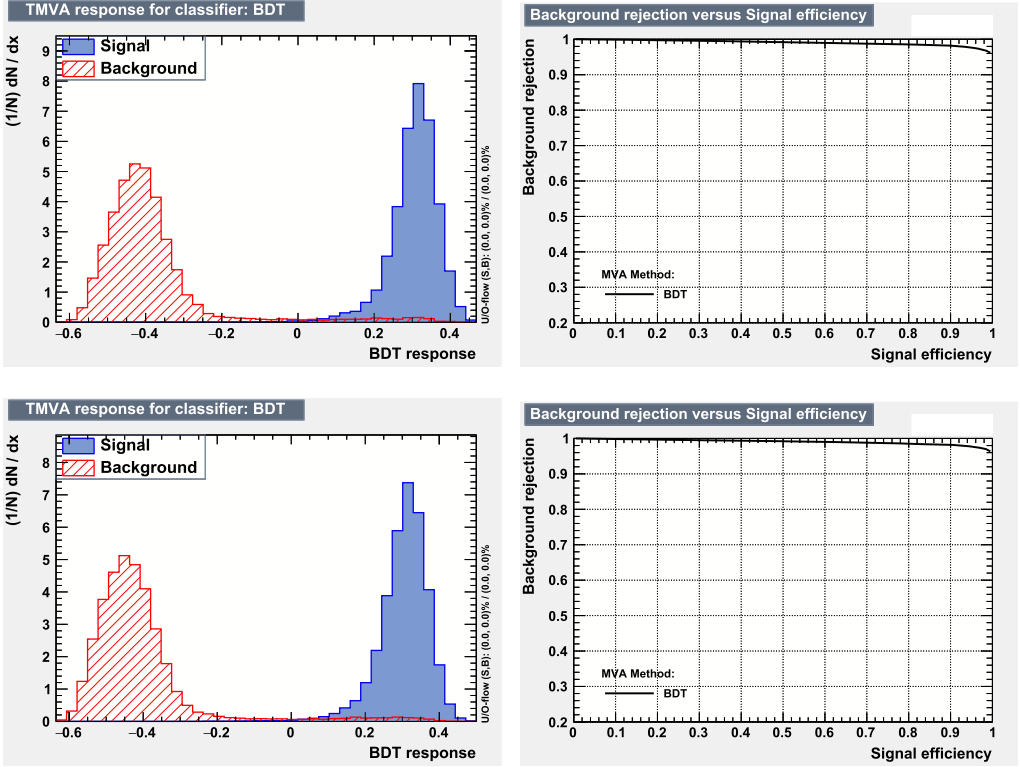
Fig. 5. Upper panels: Normalized BDT output (left) and receiver operator characteristic (ROC) curve of the BDT (right) for the electron beam energy $E_e = 60$ GeV. Lower panels: same as the upper panels but with $E_e = 120$ GeV.

leptons; $\Delta\eta^{jj}$ and $\Delta\eta^{j\ell}$; $\not{E}$, m_{jj}, and $m_{jj\ell}$. The BDT output and receiver operator characteristic (ROC) curves in Fig. 5 signify an improved separation of the signal and background. The resulting signal significances are 1.3σ and 1.2σ, respectively for 60 GeV and 120 GeV electron beams.

3.3.3. ZZ

The ZZ-to-four-lepton channel plays an important role in the discovery of Higgs boson and the measurement of its properties. Here we focus on the muonic Z decay to extract the Higgs photo-production process. This helps to exclude huge QCD backgrounds and avoid the smear from the scattered electron. There are two same-flavor and opposite-sign (SFOS) lepton pairs from ZZ decay, which leads to the invariant mass of one SFOS pair $m_{\ell\bar{\ell}}$ around m_Z, and the total invariant mass $m_{4\ell}$ close to m_h. At the meantime, the rapidity difference between the paired leptons should be small. After the lepton basic cut, the two SFOS leptons with invariant mass $^1m_{\ell\bar{\ell}}$ closest to the Z-boson mass are chosen as the first lepton pair. The requirement on $^1m_{\ell\bar{\ell}}$ is $60 \leq {^1m_{\ell\bar{\ell}}} \leq 95$ GeV. The two remaining leptons form the second lepton pair, whose invariant mass should satisfy $^2m_{\ell\bar{\ell}} \leq 60$ GeV. Since this process starts with an ergodic pairing, the background lepton-pair mass could possibly mimic the signal with a slightly broader distribution around m_Z. Even so, the $m_{4\ell}$ cut could still eliminate most of the background events because the background distribution is extremely flat, as shown in Fig. 6. Further kinematic requirements
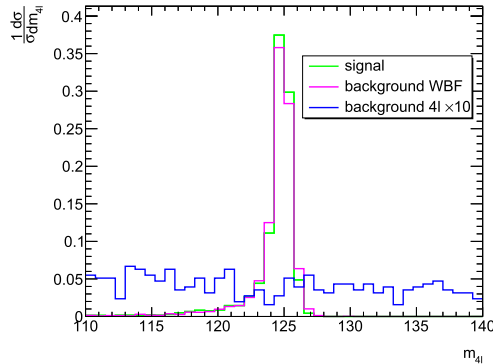
Fig. 6. $m_{4\ell}$ distributions of the signal (green), WBF background (magenta) and four-lepton background (blue). The four-lepton curve is tenfold scaled after normalization.

on lepton transverse momenta $^{1,2}p_T^\ell$ and pseudorapidity difference $^{1,2}\Delta\eta$ in the first and second lepton pairs are also used. Although with the kinematic cuts we could reduce the background to less than 1% while keep about 70% of the signal events, the huge difference between signal and background cross sections makes it impossible to perform the measurement in this channel. (The signal cross section after basic cuts is $\mathcal{O}(10^{-5})$ fb, while that of the four-lepton background is $\mathcal{O}(10^{-1})$ fb.)

4. Results and conclusion

In this paper, we study the photo-production of the Higgs boson and related contaminating processes at the LHeC. The cross sections are computed for all relevant processes. We find that the photo-production is overshadowed by other Higgs production processes whose spectator partons are collinear to one of the incoming beams and cannot be tagged.

For three dominant Higgs decay channels, we also compute their background cross sections with no Higgs produced. The signal-to-background ratios from the cut-based analysis in the previous section are $\mathcal{O}(10^{-5})$, $\mathcal{O}(10^{-2})$, and $\mathcal{O}(10^{-2})$, for the three channels $b\bar{b}$, W^+W^-, and ZZ, respectively. There is no prominent dependence of these results on the electron beam energy E_e. Signal cross sections in $b\bar{b}$ and ZZ channels are essentially negligible compared with the huge backgrounds. W^+W^- channel has an acceptable signal-to-background ratio. With the help of the BDT method to improve the cut efficiencies, the signal significances in this channel are brought up to about 1.3σ, which is still not large enough for identification of the signal in the detector.

To conclude, it is not feasible to make this complementary precision measurement for $\Gamma(h \to \gamma\gamma)$ at the LHeC using the method presented in this paper, and we hope that more discriminative methods can be developed to efficiently separate Higgs photo-production from the background processes.

CRediT authorship contribution statement

Ruibo Li: Formal analysis, Investigation, Software, Writing - original draft. **Xiang Lv:** Formal analysis, Investigation, Software, Writing - original draft. **Bo-Wen Wang:** Formal analysis, Investigation, Software, Supervision, Writing - original draft, Writing - review & editing.

Kai Wang: Conceptualization, Funding acquisition, Methodology, Resources. **Tao Xu:** Formal analysis, Investigation, Software, Writing - original draft.

Declaration of competing interest

The authors declare that they have no known competing financial interests or personal relationships that could have appeared to influence the work reported in this paper.

Acknowledgement

References

[1] ATLAS, G. Aad, et al., Observation of a new particle in the search for the Standard Model Higgs boson with the ATLAS detector at the LHC, Phys. Lett. B 716 (2012) 1–29, arXiv:1207.7214 [hep-ex].

[2] CMS, S. Chatrchyan, et al., Observation of a new boson at a mass of 125 GeV with the CMS experiment at the LHC, Phys. Lett. B 716 (2012) 30–61, arXiv:1207.7235 [hep-ex].

[3] LHeC Study Group, J.L. Abelleira Fernandez, et al., A large hadron electron collider at CERN: report on the physics and design concepts for machine and detector, J. Phys. G 39 (2012) 075001, arXiv:1206.2913 [physics.acc-ph].

[4] T. Han, B. Mellado, Higgs boson searches and the H b anti-b coupling at the LHeC, Phys. Rev. D 82 (2010) 016009, arXiv:0909.2460 [hep-ph].

[5] R. Li, B.-W. Wang, K. Wang, X. Zhang, Z. Zhou, Probing the charm Yukawa coupling at future e^-p and e^+e^- colliders, Phys. Rev. D 100 (5) (2019) 053008, arXiv:1905.09457 [hep-ph].

[6] V. Hankele, G. Klamke, D. Zeppenfeld, T. Figy, Anomalous Higgs boson couplings in vector boson fusion at the CERN LHC, Phys. Rev. D 74 (2006) 095001, arXiv:hep-ph/0609075 [hep-ph].

[7] S.S. Biswal, R.M. Godbole, B. Mellado, S. Raychaudhuri, Azimuthal angle probe of anomalous HWW couplings at a high energy ep collider, Phys. Rev. Lett. 109 (2012) 261801, arXiv:1203.6285 [hep-ph].

[8] NNPDF, R.D. Ball, V. Bertone, S. Carrazza, L. Del Debbio, S. Forte, A. Guffanti, N.P. Hartland, J. Rojo, Parton distributions with QED corrections, Nucl. Phys. B 877 (2013) 290–320, arXiv:1308.0598 [hep-ph].

[9] C. Schmidt, J. Pumplin, D. Stump, C.P. Yuan, CT14QED parton distribution functions from isolated photon production in deep inelastic scattering, Phys. Rev. D 93 (11) (2016) 114015, arXiv:1509.02905 [hep-ph].

[10] A. Manohar, P. Nason, G.P. Salam, G. Zanderighi, How bright is the proton? A precise determination of the photon parton distribution function, Phys. Rev. Lett. 117 (24) (2016) 242002, arXiv:1607.04266 [hep-ph].

[11] A.V. Manohar, P. Nason, G.P. Salam, G. Zanderighi, The photon content of the proton, J. High Energy Phys. 12 (2017) 046, arXiv:1708.01256 [hep-ph].

[12] CMS, S. Chatrchyan, et al., Exclusive photon-photon production of muon pairs in proton-proton collisions at $\sqrt{s} = 7$ TeV, J. High Energy Phys. 01 (2012) 052, arXiv:1111.5536 [hep-ex].

[13] V.M. Budnev, I.F. Ginzburg, G.V. Meledin, V.G. Serbo, The two photon particle production mechanism. Physical problems. Applications. Equivalent photon approximation, Phys. Rep. 15 (1975) 181–281.

[14] A. Buckley, J. Ferrando, S. Lloyd, K. Nordström, B. Page, M. Rüfenacht, M. Schönherr, G. Watt, LHAPDF6: parton density access in the LHC precision era, Eur. Phys. J. C 75 (2015) 132, arXiv:1412.7420 [hep-ph].

[15] R. Li, X. Lv, B.-W. Wang, K. Wang, in preparation.

[16] V. Hirschi, R. Frederix, S. Frixione, M.V. Garzelli, F. Maltoni, R. Pittau, Automation of one-loop QCD corrections, J. High Energy Phys. 05 (2011) 044, arXiv:1103.0621 [hep-ph].

[17] J. Alwall, R. Frederix, S. Frixione, V. Hirschi, F. Maltoni, O. Mattelaer, H.S. Shao, T. Stelzer, P. Torrielli, M. Zaro, The automated computation of tree-level and next-to-leading order differential cross sections, and their matching to parton shower simulations, J. High Energy Phys. 07 (2014) 079, arXiv:1405.0301 [hep-ph].

[18] T. Hahn, M. Perez-Victoria, Automatized one loop calculations in four-dimensions and D-dimensions, Comput. Phys. Commun. 118 (1999) 153–165, arXiv:hep-ph/9807565 [hep-ph].

[19] T. Hahn, CUBA: a library for multidimensional numerical integration, Comput. Phys. Commun. 168 (2005) 78–95, arXiv:hep-ph/0404043 [hep-ph].

[20] T. Sjostrand, S. Mrenna, P.Z. Skands, PYTHIA 6.4 physics and manual, J. High Energy Phys. 05 (2006) 026, arXiv:hep-ph/0603175 [hep-ph].

[21] DELPHES 3, J. de Favereau, C. Delaere, P. Demin, A. Giammanco, V. Lemaître, A. Mertens, M. Selvaggi, DELPHES 3, a modular framework for fast simulation of a generic collider experiment, J. High Energy Phys. 02 (2014) 057, arXiv:1307.6346 [hep-ex].

[22] A. Lapertosa, Calibration of the b-tagging efficiency on jets with charm quark for the ATLAS experiment, Master's thesis, Genoa U.

[23] V.D. Barger, G. Bhattacharya, T. Han, B.A. Kniehl, Intermediate mass Higgs boson at hadron supercolliders, Phys. Rev. D 43 (1991) 779–788.

[24] A. Hocker, et al., TMVA - toolkit for multivariate data analysis, arXiv:physics/0703039.